### Title

Immunotherapy-based targeting of MSLN+ activated portal fibroblasts is a strategy for treatment of cholestatic liver fibrosis




### Journal

Proceedings of the National Academy of Sciences of the United States of America, 118(29)

### ISSN

0027-8424



### Authors

Nishio, Takahiro
Koyama, Yukinori
Liu, Xiao
et al.



### Publication Date

2021-07-20

### DOI

10.1073/pnas.2101270118

Peer reviewed

# Immunotherapy-based targeting of MSLN$^+$ activated portal fibroblasts is a strategy for treatment of cholestatic liver fibrosis

Takahiro Nishio[a,b], Yukinori Koyama[d], Xiao Liu[a,b], Sara B. Rosenthal[a], Gen Yamamoto[a,b], Hiroaki Fuji[a,b], Jacopo Baglieri[a,b], Na Li[a,b,c], Laura N. Brenner[e], Keiko Iwaisako[f], Kojiro Taura[d], James S. Hagood[g], Nicholas F. LaRusso[h], Tapan K. Bera[i], Ira Pastan[i,1], David A. Brenner[a], and Tatiana Kisseleva[b,1]

[a]Department of Medicine, University of California San Diego Medical Center, La Jolla, CA 92161; [b]Department of Surgery, University of California San Diego Medical Center, La Jolla, CA 92161; [c]Shanghai University of Medicine and Health Sciences, Shanghai 201318, China; [d]Department of Surgery, Graduate School of Medicine, Kyoto University, Kyoto, 606-8501, Japan; [e]Pulmonary and Critical Care Unit, Massachusetts General Hospital and Harvard Medical School, Boston, MA 02114; [f]Department of Medical Life Systems, Faculty of Life and Medical Sciences, Doshisha University, Kyotanabe, 610-0394, Japan; [g]Program for Rare and Interstitial Lung Disease, Division of Pediatric Pulmonology, University of North Carolina at Chapel Hill, Chapel Hill, NC 27599; [h]Center for Basic Research in Digestive Diseases, Division of Gastroenterology and Hepatology, Mayo Medical School, Clinic and Foundation, Rochester, MN 55905; and [i]Laboratory of Molecular Biology, Center for Cancer Research, National Cancer Institute, NIH, Bethesda, MD 20892

Contributed by Ira Pastan, May 4, 2021 (sent for review January 26, 2021); reviewed by Yuval Rinkevich and Michael Trauner

**We investigated the role of mesothelin (Msln) and thymocyte differentiation antigen 1 (Thy1) in the activation of fibroblasts across multiple organs and demonstrated that Msln$^{-/-}$ mice are protected from cholestatic fibrosis caused by Mdr2 (multidrug resistance gene 2) deficiency, bleomycin-induced lung fibrosis, and UUO (unilateral urinary obstruction)-induced kidney fibrosis. On the contrary, Thy1$^{-/-}$ mice are more susceptible to fibrosis, suggesting that a Msln–Thy1 signaling complex is critical for tissue fibroblast activation. A similar mechanism was observed in human activated portal fibroblasts (aPFs). Targeting of human MSLN$^+$ aPFs with two anti-MSLN immunotoxins killed fibroblasts engineered to express human mesothelin and reduced collagen deposition in livers of bile duct ligation (BDL)–injured mice. We provide evidence that antimesothelin-based therapy may be a strategy for treatment of parenchymal organ fibrosis.**

cholestatic fibrosis | activated portal fibroblasts | mesothelin

Cholestatic fibrosis results from primary sclerosing cholangitis (PSC), primary biliary cirrhosis (PBC), and secondary biliary cirrhosis (SBC) caused by injury to cholangiocytes, impaired bile flow, bile accumulation (1), hepatocyte apoptosis, ductular proliferation, inflammation, and activation of myofibroblasts. The activation of both portal fibroblasts (PFs) and hepatic stellate cells (HSCs) (2) produces myofibroblasts in cholestatic diseases. Using reporter Col-GFP mice [in which collagen-1α(I) gene expression drives green fluorescent protein (GFP)], activated PFs (aPFs) were shown to comprise 70% of myofibroblasts at the onset of the bile duct ligation (BDL) model of cholestatic fibrosis, while HSCs were increasingly activated with fibrosis progression (3). Expression of thymocyte differentiation antigen 1 (Thy1), Fbln2, mesothelin (Msln), mucin 16 (Muc16), CD34, Gpc3, Asporin, and Bnc1 distinguishes Col-GFP$^+$vitaminA$^-$ aPFs from Col-GFP$^+$vitaminA$^+$Desmin$^+$GFAP$^+$–activated HSCs (aHSCs) (3).

Lineage-tracing studies by our laboratory (3, 4) and others (5) have shown that Msln-positive aPFs contribute to cholestatic fibrosis in BDL-injured or multidrug resistance gene 2 (Mdr2; Abcb4) knockout mice deficient of the canalicular phospholipid flippase (6) but not to toxic carbon tetrachloride ($CCl_4$)–induced liver fibrosis (4). In support, genetic ablation of Msln$^+$ aPFs inhibited progression of cholestatic fibrosis in adult BDL mice (4). Msln and its binding partners, Muc16 (a transmembrane-tethered mucin) (7) and Thy1 (CD90; a marker expressed by T cells, neurons, and tissue fibroblasts) (8–10), regulate a nonconventional TGFβ1–TGFβRI–Smad2/3 signaling pathway in aPFs. Msln is minimally expressed during adulthood (11, 12), which makes Msln$^+$ aPFs a target for treatment of cholestatic fibrosis.

Msln (13) and Thy1 (8) are glycosylphosphatidyl inositol (GPI)–linked membrane-anchored proteins that form a complex with Muc16 (7) in aPFs (4). Mesothelin (human counterpart, MSLN) was originally identified as a cancer-associated antigen in cancer cells from patients with mesothelioma and ovarian and pancreatic cancer, and was shown to bind the glycoprotein CA125 (human counterpart of Muc16, mouse mucin 15) (7, 14). Several different immunotherapeutic agents have been developed to treat mesothelin-expressing tumors; these include immunotoxins, antibody–drug conjugates, bispecific antibodies, and CAR-T cells (15).

Here we investigate the role of Msln, Muc16, and Thy1 in the pathogenesis of cholestatic fibrosis in Msln$^{-/-}$ mice and demonstrate that Msln$^{-/-}$ mice are protected from cholestatic fibrosis due to reduced activation of aPFs. To translate our findings to the clinic, a human liver xenograft model of cholestatic fibrosis in which primary human MSLN$^+$ aPFs are engrafted into livers of adult Rag2$^{-/-}$γc$^{-/-}$ mice was developed. Therapeutic administration of anti-human MSLN immunotoxins successfully ablated human MSLN$^+$ aPFs (>95%) and reduced collagen deposition in livers of BDL-injured mice. Our findings that Msln is expressed in some activated tissue fibroblasts and that genetic deletion of *msln* ameliorates lung (bleomycin-induced) and kidney (unilateral urinary obstruction [UUO]–induced) fibrosis in mice indicate that Msln

## Significance

**Mesothelin (Msln) expression is increased in tissue fibroblasts of damaged liver and other organs and Msln is a common mediator of liver, lung, and kidney fibrosis. We show that anti-Msln immunotoxins kill the Msln-expressing fibroblasts and reduce collagen type I deposition in fibrotic liver, indicating that agents that specifically kill Msln-expressing cells should be a useful treatment for cholestatic fibrosis. Targeting of Msln$^+$ fibroblasts by anti-Msln immunoconjugates may become a strategy for the treatment of parenchymal organ fibrosis.**

Author contributions: T.N., D.A.B., and T.K. designed research; T.N., D.A.B., and T.K. performed research; K.I., K.T., J.S.H., N.F.L., T.K.B., and I.P. contributed new reagents/analytic tools; T.N., Y.K., X.L., S.B.R., G.Y., H.F., J.B., N.L., L.N.B., and T.K. analyzed data; and T.N. and T.K. wrote the paper.

Reviewers: Y.R., Helmholtz Zentrum München; and M.T., Medizinische Universitat Wien.

The authors declare no competing interest.



[1]To whom correspondence may be addressed. Email: pastani@mail.nih.gov or tkisseleva@health.ucsd.edu.

This article contains supporting information online at https://www.pnas.org/lookup/suppl/doi:10.1073/pnas.2101270118/-/DCSupplemental.

Published July 12, 2021.

might be a common target for treatment of parenchymal organ fibrosis and immunotherapies targeting Msln$^+$ aPFs might become a strategy for treatment of cholestatic fibrosis in patients with PSC.

## Results

**Genetic Deletion of *msln* and *muc16* Suppresses Development of Cholestatic Fibrosis in Mdr2$^{-/-}$ Mice.** The role of Msln, Muc16, and Thy1 in the pathogenesis of Mdr2 deficiency–induced cholestatic fibrosis was studied in Msln$^{-/-}$Mdr2$^{-/-}$, Muc16$^{-/-}$Mdr2$^{-/-}$, and Thy1$^{-/-}$Mdr2$^{-/-}$ mice compared with Mdr2$^{-/-}$ mice. All mice were crossed with collagen-α1(I)-GFP (Col-GFP) mice to visualize fibrogenic myofibroblasts (16) (Fig. 1*A*). Cholestatic fibrosis was attenuated ∼50% in livers of Msln$^{-/-}$Mdr2$^{-/-}$ (vs. Mdr2$^{-/-}$ mice, Col-GFP$^+$C57BL/6, 12 wk old, $n$ = 10 to 12 per group; Fig. 1*B*), as shown by reduced staining areas for Sirius red (↓1.4-fold; Fig. 1*C*) and GFP$^+$Thy1$^+$ and GFP$^+$CD34$^+$ aPFs (↓2.4-fold; Fig. 1 *D* and *E* and *SI Appendix*, Fig. S1 *A–D*), and down-regulation of fibrogenic (Col1a1, αSMA, TIMP1, and TGFβ1) and aPF-specific (elastin, Thy1, fibulin-2, and CD34) genes (Fig. 1*F* and *SI Appendix*, Fig. S1*E*). Proliferation of Pan-CK$^+$ and Sox9$^+$ bile ducts was also reduced in Msln$^{-/-}$Mdr2$^{-/-}$ mice (*SI Appendix*, Fig. S1 *F–J*), suggesting that aPF activation affects the ductular reaction (17). Similar results were observed in Muc16$^{-/-}$Mdr2$^{-/-}$ mice (Fig. 1 *G–I* and *SI Appendix*, Fig. S2 *A–F*), implicating both Msln and Muc16 in mediation of profibrogenic responses in aPFs.

**Cholestatic Fibrosis Is Exacerbated in Thy1$^{-/-}$Mdr2$^{-/-}$ Mice.** In contrast to Msln$^{-/-}$Mdr2$^{-/-}$ mice, Thy1$^{-/-}$Mdr2$^{-/-}$ mice developed more fibrosis by ∼25%, which was associated with increased numbers of GFP$^+$CD34$^+$ aPFs and up-regulation of fibrogenic Col1a1, αSMA, TGFβRI, and Msln genes (but not inflammatory genes, vs. Mdr2$^{-/-}$ mice; Fig. 1 *G–I* and *SI Appendix*, Fig. S2 *G–L*) and the ductular reaction, demonstrating that Thy1 possesses antifibrogenic properties.

**Thy1 and Msln Mediate Opposing Functions in aPFs.** TGFβ1-induced Smad2 phosphorylation (p-Smad2) and αSMA protein expression were suppressed in livers of Msln$^{-/-}$Mdr2$^{-/-}$ and Muc16$^{-/-}$Mdr2$^{-/-}$ mice but increased in Thy1$^{-/-}$Mdr2$^{-/-}$ mice (compared with Mdr2$^{-/-}$ mice). Simultaneous deletion of *msln* and *thy1* eliminated the pro- and antifibrogenic responses of Msln and Thy1 in aPFs. Opposing effects of Msln and Thy1 were completely diminished in Msln$^{-/-}$Thy1$^{-/-}$Mdr2$^{-/-}$ mice to the levels observed in Mdr2$^{-/-}$ mice, as shown by total collagen deposition and expression of p-Smad2 and αSMA (*SI Appendix*, Fig. S3*A*), suggesting that Msln and Thy1 are key components of the same signaling pathway in aPFs.

**Lung and Kidney Fibrosis Is Reduced in Msln$^{-/-}$ Mice but Increased in Thy1$^{-/-}$ Mice.** To test if Msln, Muc16, and Thy1 mediate fibrogenic responses in other parenchymal organs, wild-type (WT), Msln$^{-/-}$, Muc16$^{-/-}$, Thy1$^{-/-}$, Msln$^{-/-}$Muc16$^{-/-}$, and Msln$^{-/-}$Thy1$^{-/-}$ mice (Col-GFP$^+$C57BL/6 background, 12 wk old, $n$ = 8 to 12 per group) were subjected to fibrogenic lung and kidney injury.

When challenged with a lethal dose of bleomycin (5 U/kg), ∼95% of Msln$^{-/-}$ mice survived compared with ∼25% of WT mice (vs. 100% in phosphate-buffered saline [PBS]–treated WT mice; Fig. 2*A*). Moreover, Msln$^{-/-}$ mice (Fig. 2 *B–E*) but not Muc16$^{-/-}$ mice (Fig. 2 *F* and *G*) were protected by ∼50% from bleomycin (1 U/kg, 3 wk)-induced lung fibrosis. Msln$^{-/-}$ mice had reduced activation of Col-GFP$^+$Thy1$^+$ lung fibroblasts (vs. WT mice; Fig. 2 *D* and *E*). On the other hand, Thy1$^{-/-}$ mice were more susceptible to lung fibrosis (by 25%; Fig. 2 *F–H*). Our data are in concordance with previous observations that implicated Thy1 in regulation of antifibrogenic responses in lung fibroblasts (18–20).

Similar results were observed in mice with kidney fibrosis that was surgically induced by UUO (2 wk, Col-GFP$^+$C57BL/6, 12 wk old). Kidney fibrosis was suppressed by ∼40% in Msln$^{-/-}$ mice (and was associated with reduced numbers of Col-GFP$^+$Thy1$^+$ tubular fibroblasts; Fig. 3 *A–D*) but increased by ∼25% in Thy1$^{-/-}$ mice (vs. WT mice; Fig. 3 *E–G*).

Although Muc16$^{-/-}$ mice showed somewhat improved (∼15%) survival after acute lung injury (vs. WT mice; Fig. 2*A*), Muc16$^{-/-}$ mice were not protected from either lung or kidney fibrosis (Figs. 2 *F–H* and 3 *E–G*), suggesting that unlike cholestatic fibrosis (4), Muc16 is dispensable for activation of lung and kidney fibroblasts. For this reason, inhibition of lung and kidney fibrosis in Msln$^{-/-}$Muc16$^{-/-}$ mice was attributed to Msln deficiency in tissue fibroblasts.

Analogous to cholestatic fibrosis (Fig. 1 *G–I*), Msln$^{-/-}$Thy1$^{-/-}$ mice with bleomycin (Fig. 2 *F* and *G* and *SI Appendix*, Fig. S3 *B* and *D*) or UUO injury (Fig. 2 *E* and *F* and *SI Appendix*, Fig. S3 *C* and *E*) developed a phenotype similar to that in WT mice, suggesting that Msln and Thy1 mediate opposing functions in lung and kidney fibroblasts, suggesting that a similar mechanism regulates activation of tissue fibroblasts.

**Gene Expression Profiles Are Similar in aPFs and Lung and Kidney Fibroblasts.** Primary aPFs and lung and kidney tubular fibroblasts were isolated and their gene expression profiles were compared by RNA sequencing (RNA-seq).

Specifically, GFP$^+$vitaminA$^-$ aPFs were sort-purified (from GFP$^+$vitamin A$^+$ aHSCs and GFP$^-$vitamin A$^+$ quiescent HSCs [qHSCs]; *SI Appendix*, Figs. S4 and S5) from livers of Mdr2$^{-/-}$, Msln$^{-/-}$Mdr2$^{-/-}$, Muc16$^{-/-}$Mdr2$^{-/-}$, and Thy1$^{-/-}$Mdr2$^{-/-}$ mice (Col-GFP$^+$C57BL/6, 12 wk old, $n$ = 4 to 6 per group) (3), and analyzed by RNA-seq. A strong separation in expression of "liver fibrosis–associated" genes distinguished aPFs of different genotypes (DisGeNet; Fig. 4*A* and *SI Appendix*, Fig. S6 *A–F*). Msln-deficient aPFs exhibited a defect in activation, while Thy1-deficient aPFs up-regulated expression of the fibrogenic genes Col1a1, Col1a2, and αSMA (Fig. 4*B*). Among all genes significantly altered in the knockout vs. WT aPFs, Msln$^{-/-}$Mdr2$^{-/-}$ and Thy1$^{-/-}$Mdr2$^{-/-}$ aPFs shared more similarities within fibrogenic pathways (dysregulated in opposite directions) than Msln$^{-/-}$Mdr2$^{-/-}$ and Muc16$^{-/-}$Mdr2$^{-/-}$ aPFs (vs. Mdr2$^{-/-}$ aPFs), indicating that Muc16 functions are not limited to TGFβ1/TGFβRI signaling in aPFs (Fig. 4*C* and *SI Appendix*, Fig. S6).

Col-GFP$^+$Thy1$^+$ lung and kidney fibroblasts were sort-purified from bleomycin- or UUO-injured WT and Msln$^{-/-}$ mice (Col-GFP$^+$C57BL/6, 12 wk old, $n$ = 4 to 6 per group; *SI Appendix*, Fig. S7*A*) and analyzed by qRT-PCR (*SI Appendix*, Fig. S7*B*) and RNA-seq (*SI Appendix*, Figs. S7 *C–E* and S8). Comparison of the top 500 most expressed genes revealed similarities between aPFs and lung and kidney fibroblasts (Fig. 4*D*), which share expression of common markers (Msln, Thy1, Gremlin1, Calca, Upk1b, Fbln1, CD34, Asporin, Gpc3, Bnc1, and CD200; Fig. 4*E*). Moreover, Msln$^{-/-}$ lung and kidney fibroblasts down-regulated expression of fibrogenic genes (Col1a1, Timp1, Spp1, TGFβRI, Smad2/3, and vimentin vs. WT fibroblasts; Fig. 4*F*) in the same way as Msln$^{-/-}$ aPFs and exhibited consistent gene up/down-regulation compared with Msln$^{-/-}$ aPFs (Fig. 4*G*). Thus, among the 43 genes commonly down-regulated in Msln$^{-/-}$ aPFs and lung and kidney fibroblasts, 18 genes (including Msln, MMP3/10, Ccl7, Cxcl1/12/14, IL1β, Sparcl1, Penk, Bmp2, and FGF7) mediate specific functional processes (Fig. 4*H*), indicating that Msln has similar biological functions in aPFs and lung and kidney fibroblasts.

**Msln and Thy1 Regulate TGFβ/TGFβRI Signaling in aPFs and Lung Fibroblasts.** Primary aPFs (Mdr2$^{-/-}$, Msln$^{-/-}$Mdr2$^{-/-}$, and Thy1$^{-/-}$Mdr2$^{-/-}$) and Thy1$^+$ lung fibroblasts (WT, Msln$^{-/-}$, and Thy1$^{-/-}$) were cultured ±TGFβ1 (5 ng/mL, for 30 min). Expression of TGFβ1-mediated p-Smad2, p-Akt, αSMA, and TGFβRI proteins was down-regulated in Msln$^{-/-}$ aPFs and lung fibroblasts but increased in Thy1$^{-/-}$ aPFs (Fig. 5 *A* and *B*). Deletion of *thy1* in aPFs was associated with strong overexpression of Msln protein

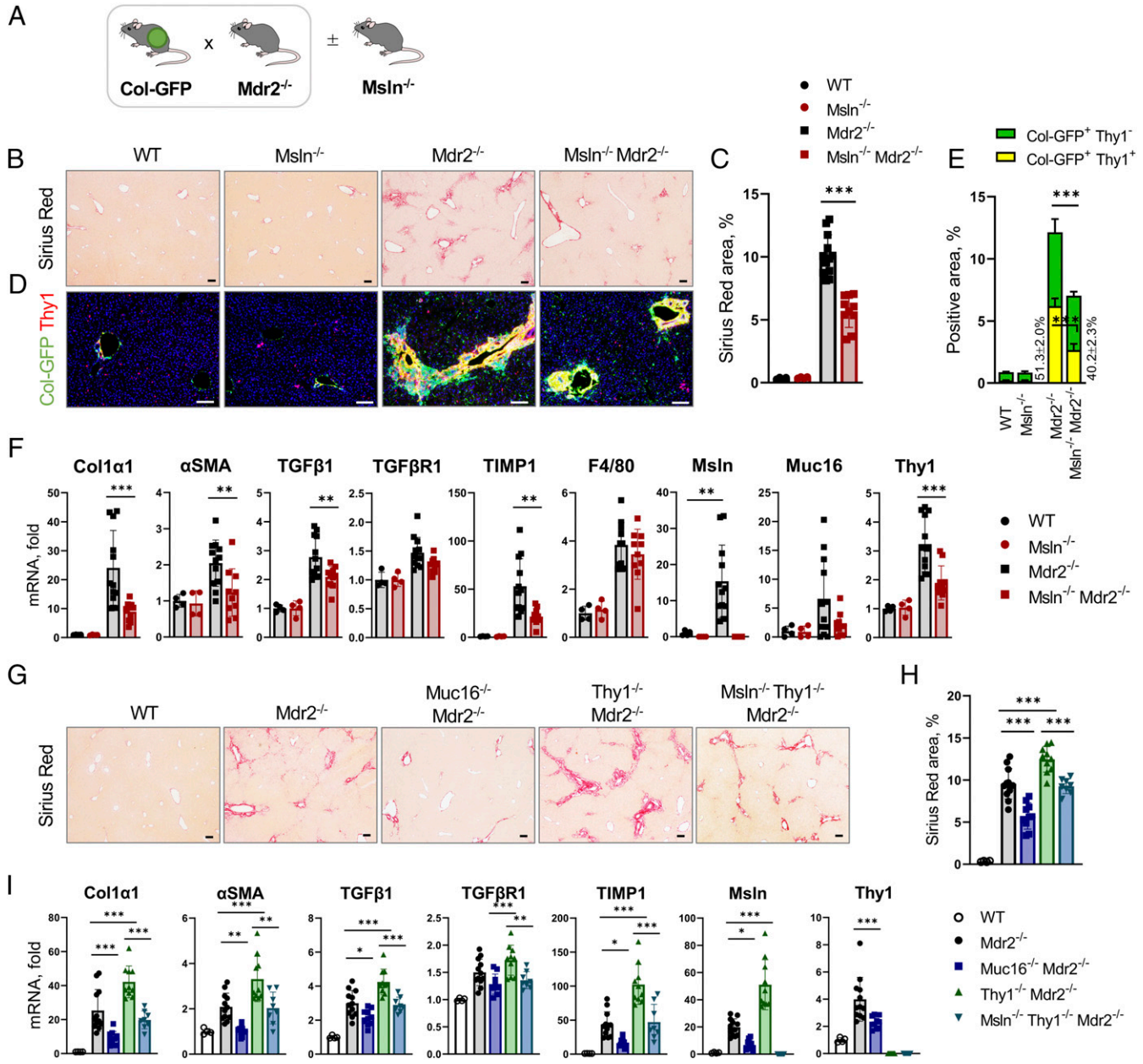


**Fig. 1.** *Mdr2* deficiency–induced cholestatic fibrosis is reduced in Msln$^{-/-}$ and Muc16$^{-/-}$ mice but increased in Thy1$^{-/-}$ mice. (*A*) Experimental outline: Mdr2$^{-/-}$Col-GFP mice were crossed ±Msln$^{-/-}$ mice, mice were killed at 12 wk of age, and development of cholestatic fibrosis was analyzed. (*B* and *C*) Livers were stained with Sirius red (*B*), and the positive area was calculated as a percentage (*C*). (*D*) Livers were stained for Thy1 to visualize GFP$^{+}$ aPFs. (*E*) Area of the overlapping Thy1$^{+}$GFP$^{+}$ staining was calculated as a percentage (vs. total GFP$^{+}$ area, 100%). (*F*) Expression of fibrogenic (Col1α1, αSMA, Desmin, TGFβ1, TIMP1) genes and macrophage-specific (F4/80) and aPF markers (Msln, Muc16, Thy1) was assessed by qRT-PCR. (*G–I*) Livers of Mdr2$^{-/-}$, Muc16$^{-/-}$Mdr2$^{-/-}$, Thy1$^{-/-}$Mdr2$^{-/-}$, and Msln$^{-/-}$Thy1$^{-/-}$Mdr2$^{-/-}$ mice were analyzed. (*G* and *H*) Livers were stained with Sirius red (*G*), and the positive area was calculated as a percentage (*H*). (*I*) Expression of selected genes was analyzed by qRT-PCR. (Scale bars, 100 μm.) Mean ± SD. *$P < 0.05$, **$P < 0.01$, and ***$P < 0.001$ by ANOVA.

(↑8-fold; Fig. 5 *A* and *B*) and messenger RNA (mRNA) (↑2.3-fold; Figs. 1*I* and 2*H*), indicating that Thy1 might negatively regulate the Msln signaling pathway. In turn, expression of TGFβRI protein (Fig. 5 *A* and *B*) but not mRNA (Fig. 1*F*) was suppressed in Msln-deficient aPFs, suggesting that Msln might affect TGFβRI protein stability.

A series of immunoprecipitations (IPs)/Western blots was performed on aPFs (Mdr2$^{-/-}$ and Msln$^{-/-}$Mdr2$^{-/-}$) and Col-GFP$^{+}$ lung fibroblasts (WT and Msln$^{-/-}$) using anti-Msln, anti-Muc16, and anti-TGFRI antibodies (Abs), and revealed the dynamic interaction between Msln–Muc16 and Msln–Thy1 in TGFβ1-stimulated aPFs (Fig. 5*C*) but not between Msln–TGFRI or Muc16–Thy1 (Fig. 5 *D* and *E*). We propose that under physiological conditions, Thy1 forms an inhibitory complex with TGFβRI (Fig. 5*F*). TGFβ1 stimulation facilitates the binding between Msln and Thy1, thereby promoting dissociation of Thy1 from TGFβRI and enabling TGFβ1/TGFβRI signaling (Fig. 5*F*). Taken together, formation of the Thy1–Msln complex regulates TGFβ1/TGFβRI signaling not only in aPFs but also in lung fibroblasts. Although Msln binding to Muc16 was observed in both aPFs and lung fibroblasts (Fig. 5 *C* and *E*), functional significance of the Msln–Muc16 complex for stimulation of TGFβ1/TGFβRI signaling was shown only in aPFs

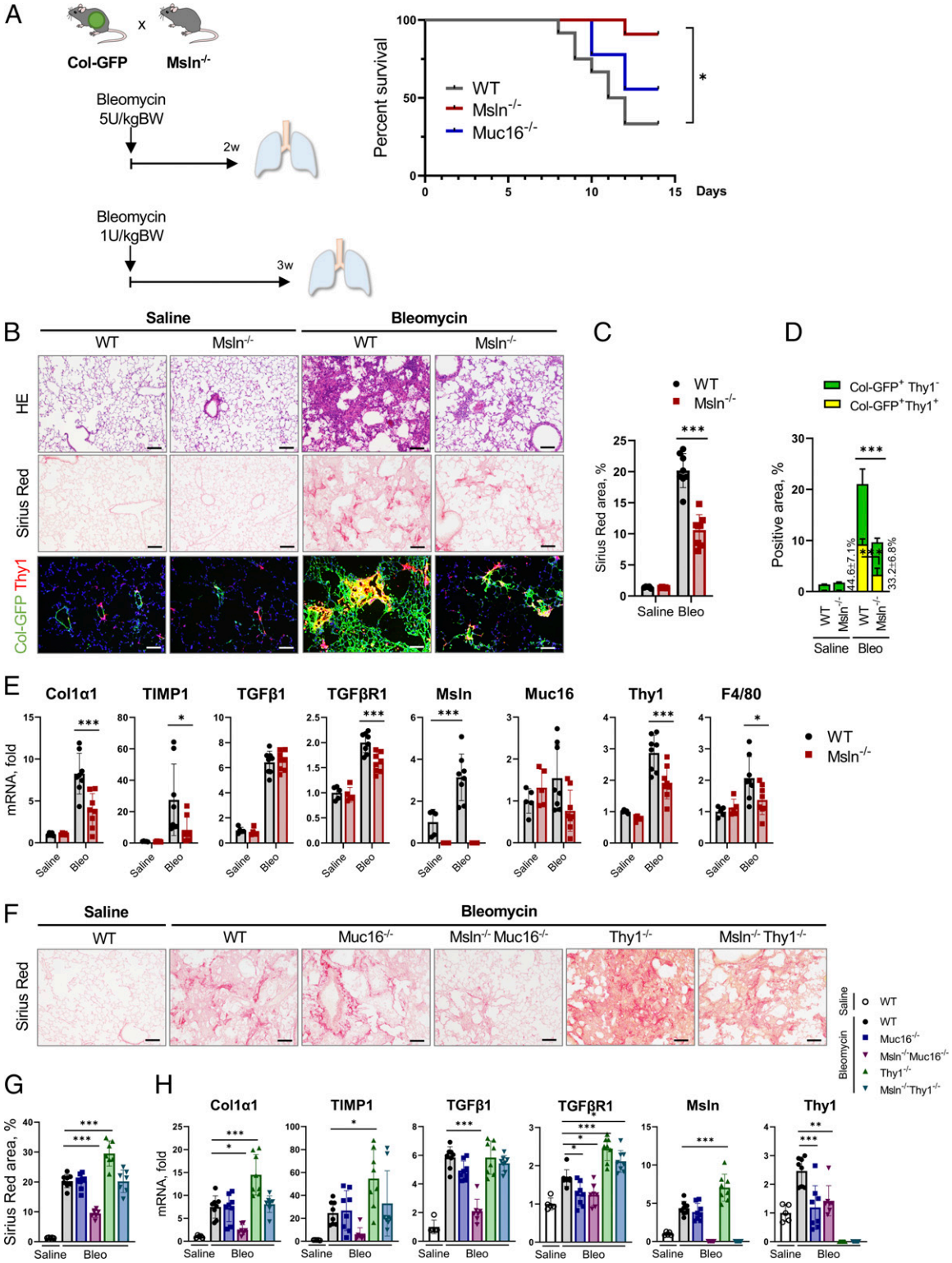


**Fig. 2.** Lung fibrosis is attenuated in Msln$^{-/-}$ mice but increased in Thy1$^{-/-}$ mice. (*A*) Col-GFP mice were crossed ±Msln$^{-/-}$ mice (or ±Muc16$^{-/-}$ mice), treated with bleomycin (5 U/kg), and monitored for 2 wk. Survival rate was calculated using the Kaplan–Meier method. BW, body weight. (*B–E*) Col-GFP and Msln$^{-/-}$Col-GFP mice were treated with bleomycin (1 U/kg, 3 wk, or PBS). (*B*) Lungs were stained with H&E, Sirius red, or anti-Thy1 Ab. (*C* and *D*) Positive area of Sirius red staining (*C*), or Thy1$^{+}$GFP$^{+}$ fibroblasts (vs. total GFP$^{+}$ fibroblasts) was calculated as a percentage (*D*). (*E*) Expression of fibrogenic, macrophage-specific, and aPF markers was analyzed by qRT-PCR. (*F–H*) WT, Muc16$^{-/-}$, Msln$^{-/-}$Muc16$^{-/-}$, Thy1$^{-/-}$, and Msln$^{-/-}$Thy1$^{-/-}$ mice were treated with bleomycin (1 U/kg, 3 wk) or PBS. (*F*) Lungs were stained with Sirius red. (*G*) The positive area was calculated as a percentage. (*H*) Expression of selected genes was analyzed by qRT-PCR. (Scale bars, 100 μm.) Mean ± SD. *$P < 0.05$, **$P < 0.01$, and ***$P < 0.001$ by ANOVA.

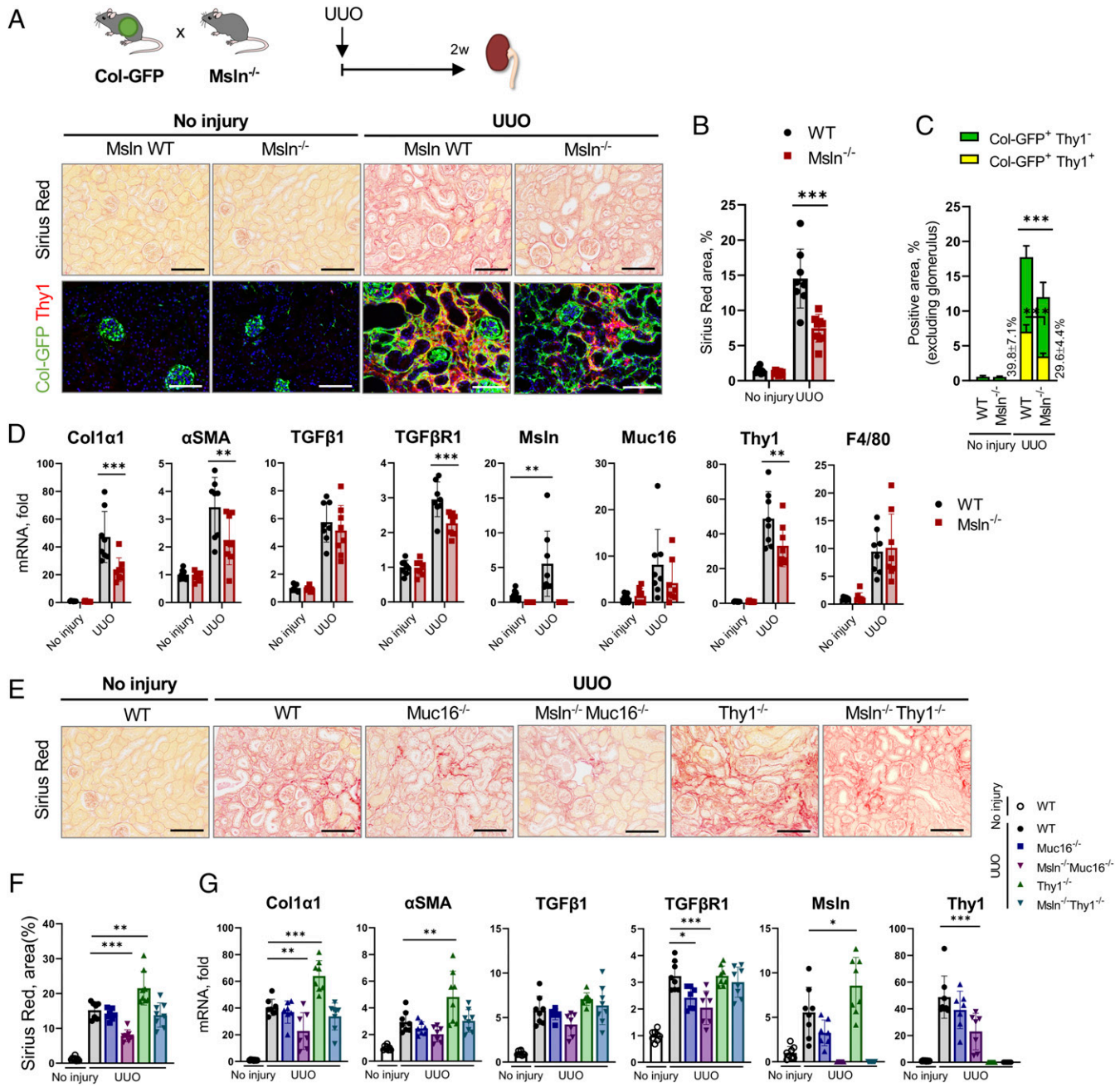


**Fig. 3.** Kidney fibrosis is attenuated in Msln$^{-/-}$ mice but exacerbated in Thy1$^{-/-}$ mice. (*A–D*) Col-GFP mice were crossed ±Msln$^{-/-}$ mice and subjected to UUO (2 wk). (*A*) Injured and contralateral (control) kidneys were stained with Sirius red and anti-Thy1 Ab. (*B* and *C*) Positive area of Sirius red (*B*) and Thy1$^{+}$GFP$^{+}$ fibroblasts (vs. total GFP$^{+}$ fibroblasts) was calculated as a percentage (*C*). (*D*) Expression of selected genes was analyzed by qRT-PCR. (*E–G*) Kidneys from UUO-injured WT, Muc16$^{-/-}$, Msln$^{-/-}$Muc16$^{-/-}$, Thy1$^{-/-}$, and Msln$^{-/-}$Thy1$^{-/-}$ mice were stained with Sirius red (*E*), the positive area was calculated as a percentage (*F*), and expression of selected genes was analyzed by qRT-PCR (*G*). (Scale bars, 100 μm.) Mean ± SD. *$P < 0.05$, **$P < 0.01$, and ***$P < 0.001$ by ANOVA.

(Fig. 1 *G–I*) (4) but may play a limited role in the pathogenesis of bleomycin-induced (or UUO-induced) fibrosis (Figs. 2 *F* and *G* and 3 *E* and *F*).

**Binding Partners of Msln Affect Cholestatic Fibrosis.** Muc16 is the only known Msln ligand (21). Searching for potential novel Msln-binding partners, we performed curator-evaluated computational STRING analysis. Based on experimental findings in different tissues and cell types, binding of Msln and Thy1 to the Psca–Nrn1–Nfm complex was linked to Muc16–(Muc3/4/5/6/13/15) glycoproteins (Fig. 5*G*). Msln and Thy1 also interact with two groups of proteins (Gpc3, IL6, Fn1, Spp1, Eng, CD34, Alpi, and Itgam; and Cecam5, Psca, Folr2, CD109, Negr1, Nm1, and Ly6d/e), some of which were identified as aPF-specific markers (Fig. 5*H*). Moreover, formation of Msln–(Rala–Zbtt–Rnn) and Thy1–(Sco1/2–Sugp1/2–Ube2i–Ubl4–Mrpl53) complexes were linked to phosphatidylinositol glycan–specific phospholipase D1 hydrolysis of GPI anchors from protein-curated pathways (22) (Fig. 5*I*), suggesting that Msln and Thy1 (but not Muc16) might coregulate Ndufa2/6/8–Ndufb5/6/9–Ndufs1/5 proteins. In support, RNA-seq analysis revealed that expression of NADH ubiquinone oxidoreductase (Nduf) genes was strongly reduced in Msln$^{-/-}$, Muc16$^{-/-}$,

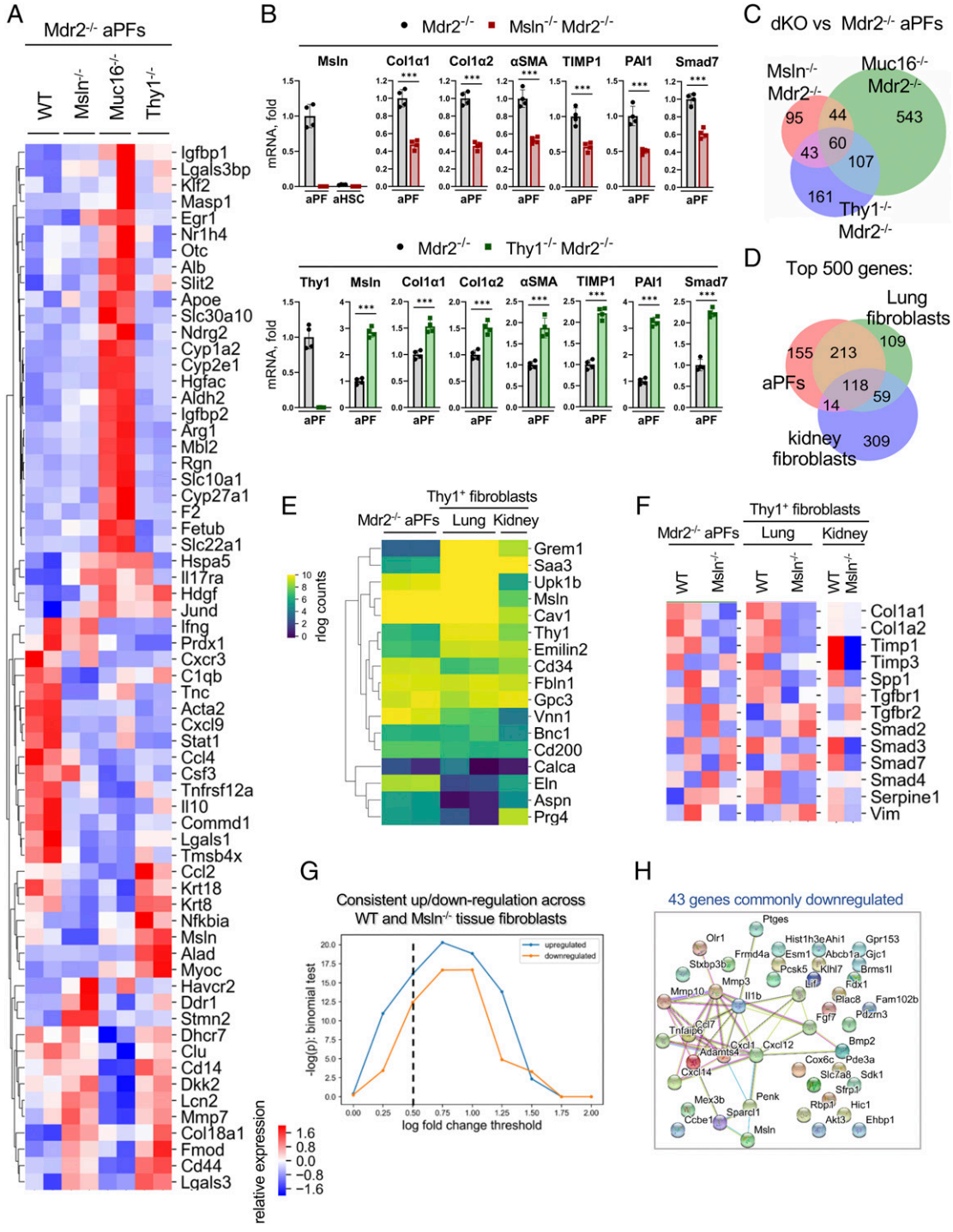


**Fig. 4.** aPFs share similarities with activated lung and kidney fibroblasts. (*A*–*C*) Sort-purified primary Msln$^{-/-}$Mdr2$^{-/-}$Col-GFP$^{+}$, Muc16$^{-/-}$Mdr2$^{-/-}$Col-GFP$^{+}$, and Thy1$^{-/-}$Mdr2$^{-/-}$Col-GFP$^{+}$ aPFs compared with Mdr2$^{-/-}$Col-GFP$^{+}$ (control; two independent sorts, >3 mice per group) using RNA-seq. (*A*) Heatmap shows relative expression of dysregulated genes in aPFs (false discovery rate [FDR] < 0.2) which are associated with liver fibrosis (DisGeNet). (*B*) Expression of selected genes was confirmed by qRT-PCR. Mean ± SD. ***$P < 0.001$ by unpaired Student's *t* test. (*C*) Venn diagram depicts similarities and differences between double-knockout (dKO) Msln$^{-/-}$Mdr2$^{-/-}$, Thy1$^{-/-}$Mdr2$^{-/-}$, and Muc16$^{-/-}$Mdr2$^{-/-}$ mice (vs. Mdr2$^{-/-}$ aPFs; FDR < 0.2). (*D* and *E*) Col-GFP$^{+}$Thy1$^{+}$ lung and kidney fibroblasts were sort-purified from WT or Msln$^{-/-}$Col-GFP mice with bleomycin-injured lung (two independent sorts, >3 mice per group) and UUO-injured kidney (>3 mice per group), respectively. Comparison of the top 500 expressed genes in Mdr2$^{-/-}$ aPFs and Col-GFP$^{+}$Thy1$^{+}$ lung and kidney fibroblasts. (*D*) Venn diagram showing an overlap of the most highly expressed genes. (*E*) Expression of aPF-specific genes is shown (rlog normalized counts). (*F*–*H*) Comparison of Msln$^{-/-}$Mdr2$^{-/-}$ aPFs and Msln$^{-/-}$Thy1$^{+}$ lung and Msln$^{-/-}$Thy1$^{+}$ kidney fibroblasts. (*F* and *G*) Msln-deficient aPFs and lung and kidney fibroblasts down-regulate expression of TGFβ1-responsive genes. Relative expression is shown (*F*), and shows more genes consistently up-regulated and down-regulated across aPFs and lung and kidney fibroblasts than expected by chance (*G*) (vs. Mdr2$^{-/-}$ aPFs and WT Thy1$^{+}$ lung and WT Thy1$^{+}$ kidney fibroblasts; binomial test *P* value for the number of genes observed commonly up- and down-regulated as a function of log fold-change threshold). (*H*) The interconnections between 43 commonly down-regulated genes at log fold change <−0.5 were identified using a cross-species protein–protein interaction network. Genes have more connections than expected by chance ($P < 1E-16$, permutation test), suggesting they belong to common underlying pathways.

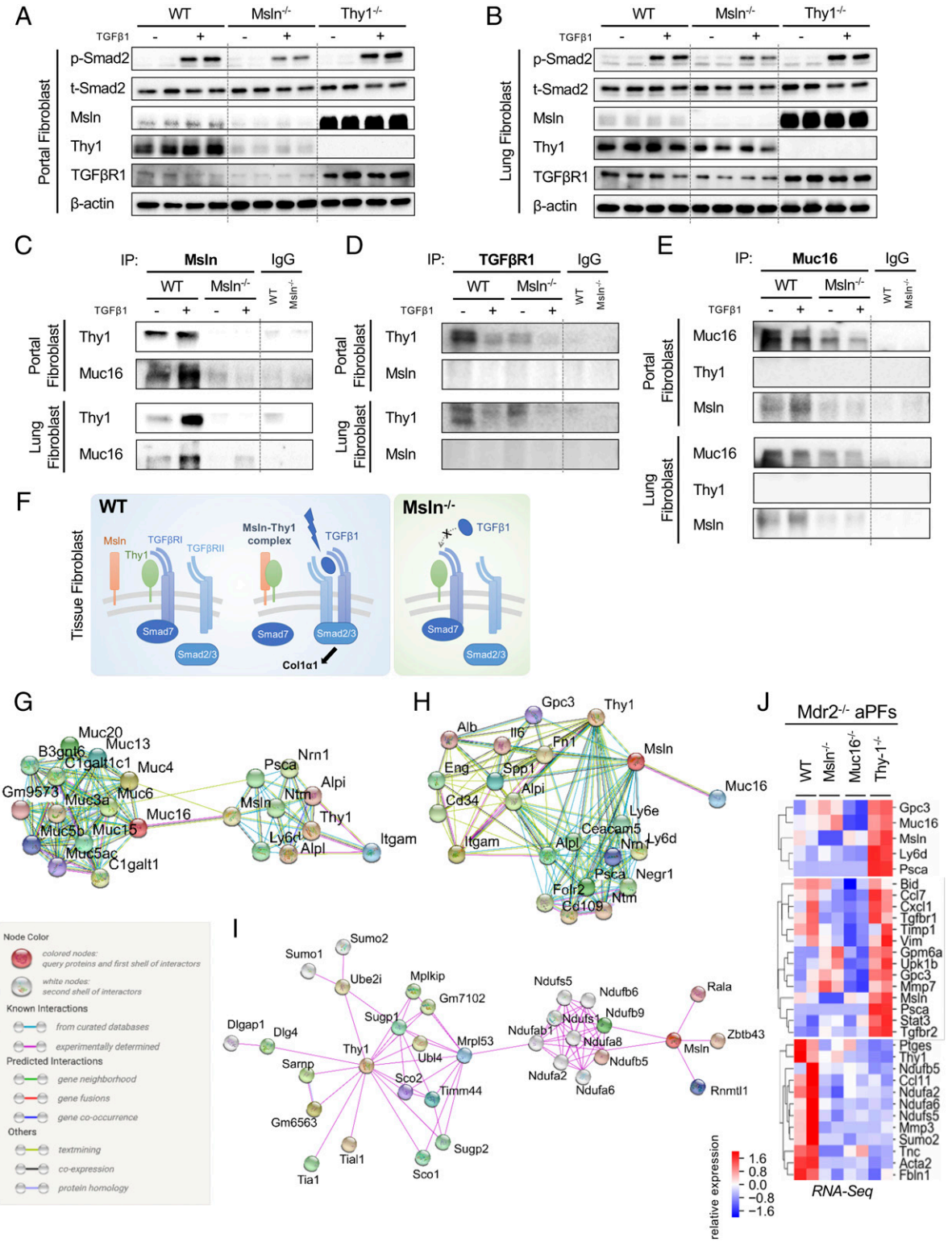


**Fig. 5.** Msln regulates similar responses in aPFs and lung fibroblasts. (*A*–*E*) Responses to ±TGFβ1 (5 ng/mL, for 30 min) were compared in aPFs (Mdr2$^{-/-}$, Msln$^{-/-}$Mdr2$^{-/-}$, and Thy1$^{-/-}$Mdr2$^{-/-}$) (*A*) and activated lung fibroblasts (WT, Msln$^{-/-}$, and Thy1$^{-/-}$) (*B*) using Western blotting for phospho-Smad2/Smad2, Msln, Thy1, and TGFβRI (normalized to the levels of β-actin expression), or IPs with anti-Msln Ab (*C*), anti-TGFβRI Ab (*D*), and anti-Muc16 Ab (vs. IgG) (*E*). (*F*) Proposed model of Msln–Thy1–TGFβRI signaling in tissue fibroblasts (see explanations in the text). (*G*–*J*) STRING network analysis depicts the top 20 first-neighbor genes connecting Msln–Thy1 (*G*) and Muc16–Msln (*H*). Known (shown with turquoise and purple connecting lines), predicted (green, red, and blue lines), or other (lime, black, and dark blue lines) interactions are shown. (*I*) Top 30 first- and second-neighbor genes connecting Msln–Thy1, experimentally determined interactions only. (*J*) RNA-seq–based relative expression of selected genes in Mdr2$^{-/-}$, Msln$^{-/-}$Mdr2$^{-/-}$, Muc16$^{-/-}$Mdr2$^{-/-}$, and Thy1$^{-/-}$Mdr2$^{-/-}$ aPFs is shown.

and Thy1$^{-/-}$ aPFs, implying that Msln–Thy1–Muc16 signaling might mediate mitochondrial respiration and adenosine triphosphate synthesis pathways in aPFs (Fig. 5*J*). In addition, increased amino acid/lipid biosynthesis was detected in Muc16$^{-/-}$ aPFs (vs. WT, Msln$^{-/-}$, or Thy1$^{-/-}$ aPFs), implicating Muc16 in suppression of metabolic processes in aPFs (*SI Appendix*, Fig. S9). As a proof of principle, extracellular matrix/collagen pathways were dysregulated in opposite directions in Msln$^{-/-}$ and Thy1$^{-/-}$ aPFs (*SI Appendix*, Fig. S9).

**Expression of Msln and Thy1 Is Up-Regulated in Livers of PSC Patients.** To translate our findings, human livers from PSC patients (stage 2, $n = 5$; stage 4, $n = 10$; and control, $n = 5$) were analyzed by immunohistochemistry. We observed a correlation between expression of human MSLN and THY1 and the stage of liver fibrosis, suggesting that MSLN might become a target for antifibrotic therapy (Fig. 6 *A* and *B* and *SI Appendix*, Fig. S10 *A* and *B*). In support, human aPFs were isolated from donor livers with cholestasis ($n = 6$, declined for transplantation; https://www.lifesharing.org) and analyzed by immunocytochemistry, qRT-PCR, and RNA-seq. Human MSLN$^+$THY1$^+$αSMA$^+$ aPFs (*SI Appendix*, Fig. S10*C*) expressed aPF-specific markers (UPK1b, CD200, EMILIN2, BNC1, ASPN, GPC3, and GREM1; Fig. 6*C* and *SI Appendix*, Fig. S10*D*), similar to that observed in mouse aPFs (Fig. 6*D* and *SI Appendix*, Fig. S10*E*) (3), and up-regulated COL1a1, αSMA, TIMP1, PAI1, SMAD7, and TGFβ1 when stimulated with TGFβ1 (5 ng/mL) ±Alk5 inhibitor (SB431542, 10 μM, 24 h; *SI Appendix*, Fig. S10*F*).

**Immunotherapy-Based Strategy to Target Human aPFs.** We have demonstrated that genetic ablation of aPFs attenuates development of cholestatic fibrosis in BDL-injured mice (4). We hypothesized that immunotoxin-based ablation of human aPFs may become a strategy for treatment of PSC patients. Several generations of immunotoxins, such as SS1P and LMB-100, were engineered by attachment of an anti-human MSLN SS1 Ab (23, 24) to PE38 toxin (truncated *Pseudomonas* exotoxin that causes cellular apoptosis via inactivation of the adenosine diphosphate ribosylation/elongation factor 2 pathway) (25). SS1P and LMB-100 have been tested in clinical trials in patients with mesothelioma and ovarian and pancreatic cancer (26–29). Using fluorescent labeling of SV40-large T antigen-GFP adenovirus (4), we tested the ability of SS1P and/or LMB-100 to kill human aPFs in vitro and in vivo (*SI Appendix*, Fig. S10).

**Administration of Anti-MSLN Ab Immunotoxin Resulted in Ablation of Human aPFs and Suppression of Cholestatic Fibrosis in Recipient Rag2$^{-/-}$γc$^{-/-}$ Mice.** SS1P and LMB-100 (0.05 to 100 ng/mL, 72 h) killed 70 to 80% of human aPFs in vitro, compared with anti–transferrin receptor immunotoxin HB-21-Fv-PE40 (100%, positive control; Fig. 6 *E* and *F*).

Furthermore, xenograft Rag2$^{-/-}$γc$^{-/-}$ mice were generated by transplantation of human GFP$^+$MSLN$^+$ aPFs ($1 \times 10^6$ cells) into the livers of immunodeficient mice (12 wk old, BalbC, $n = 5$ to 8 per group; Fig. 6*G*) and subjected to BDL (Fig. 5*D*). On days 1 and 3 post BDL, xenograft Rag2$^{-/-}$γc$^{-/-}$ mice were intravenously (i.v.) injected with SS1P (100 μg/kg) or vehicle (0.2% human serum albumin). Administration of SS1P to the xenograft Rag2$^{-/-}$γc$^{-/-}$ mice resulted in successful ablation of human aPFs, as shown by disappearance of GFP$^+$ aPFs in immunotoxin-treated mice (vs. vehicle-treated mice; Fig. 6 *H–J* and *SI Appendix*, Fig. S11*A*) (29).

Specifically, human aPFs proliferated within the left lateral lobe, migrated to the portal areas, up-regulated αSMA and MSLN (Fig. 6*K* and *SI Appendix*, Fig. S11*B*), and contributed to cholestatic fibrosis. A noninjected median lobe served as a negative control as it did not engraft human aPFs (*SI Appendix*, Fig. S11*C*). Remarkably, disappearance of GFP$^+$ aPFs in immunotoxin-treated mice was associated with decreased BDL-induced fibrosis in the left lateral lobe (transplanted with human aPFs, but not in the median lobe; Fig. 6 *H–L*), as shown by the decreased area of Sirius red staining (Fig. 6*I*) and reduced expression of Col1a1, αSMA, and Thy1 mRNA (Fig. 6*L*). Overall, immunotherapy-based targeting of human MSLN$^+$ aPFs might provide a strategy for the treatment of cholestatic fibrosis.

## Discussion

Here we investigate the role of Msln, Muc16, and Thy1 in fibrosis and fibroblast activation across multiple organs and demonstrate that Msln$^{-/-}$ mice are protected from cholestatic fibrosis caused by Mdr2 deficiency, bleomycin-induced lung fibrosis, and UUO-induced kidney fibrosis. We propose that Msln is a critical activator of tissue fibroblasts. Msln expression correlated with the stage of liver fibrosis in patients with PSC. Anti-MSLN immunotoxins, developed for cancer therapy, were used to target human MSLN$^+$ aPFs in vitro and in vivo. We demonstrate that SS1P and LMB-100 immunotoxins can successfully kill human aPFs, suggesting that immunotherapy-based targeting of MSLN$^+$ tissue fibroblasts might provide a strategy for treatment of parenchymal organ fibrosis.

HSCs have been well-characterized as the pericytes of the liver (30), which reside in the space of Disse, store vitamin A, and are activated in response to a variety of hepatotoxic injuries including viral hepatitis, alcoholic liver disease, and nonalcoholic steatohepatitis (2). On the other hand, PFs are distinctively identified as liver-resident fibroblasts surrounding the biliary component, which comprise a population of 0.1% of total liver cells and physiologically maintain the integrity of the portal tract (2). PFs get activated and proliferate around the portal area, responding to biliary obstruction and damage. Accordingly, aPFs serve as a significant source of collagen-α1(I)–producing myofibroblasts in cholestatic liver fibrosis, such as biliary atresia, PBC, or PSC (1, 3, 31). In accordance, a critical role of aPFs in the pathogenesis of cholestatic injury was shown using BDL-injured mice and Mdr2$^{-/-}$ mice [also known as Abcb4$^{-/-}$ mice (6)], a well-established experimental model of cholestatic fibrosis that spontaneously develops pericholangitis and biliary fibrosis and resembles the pathology of human PSC (32). Here we demonstrate that the number of aPFs was strongly reduced in Msln$^{-/-}$Mdr2$^{-/-}$ mice and was associated with suppression of cholestatic fibrosis in these mice, confirming that Msln is an important activator of aPFs.

Msln expression is abundant in normal mesothelial cells, which are the components of the mesothelial layer lining parenchymal organs and serosal cavities (11). Tissue-resident fibroblasts reside in the interstitium in a quiescent state and generally comprise a minor mesenchymal population in any normal tissue. In response to tissue injury or stress, tissue fibroblasts get activated, proliferate, and differentiate into myofibroblasts. Tissue fibroblasts as well as pericytes can serve as major myofibroblast precursors in various organ fibrotic diseases, including not only liver but also kidneys and lungs (33, 34). Based on the functional link between Msln expression and activation of aPFs, we hypothesized that there are similar fibroblast populations in multiple organs, which may become activated via a common Msln–Thy1–mediated signaling cascade to differentiate into matrix-producing activated myofibroblasts. Indeed, aPFs and activated lung and kidney fibroblasts share similarities, and express common markers (Msln, Thy1, Gremlin1, Calca, Upk1b, Fbln1, CD34, Asporin, Gpc3, Bnc1, and CD200) as well as recently identified markers of peribiliary mesenchymal cells (Gli1/2, Osr1, Mfap5, and Vit; *SI Appendix*, Fig. S7*E*) (35, 36). Similar to cholestatic fibrosis, Msln$^{-/-}$ mice are protected from lung and kidney fibrosis, while Thy1$^{-/-}$ mice are more susceptible to fibrosis, suggesting that Msln–Thy1 signaling plays a key role in activation of tissue fibroblasts.

In support, simultaneous deletion of *msln* and *thy1* genes yielded a phenotype similar to that in WT littermates, indicating that Msln and Thy1 might regulate opposing functions within one signaling pathway. Thy1 was implicated in inhibition of TGFβ1 signaling in

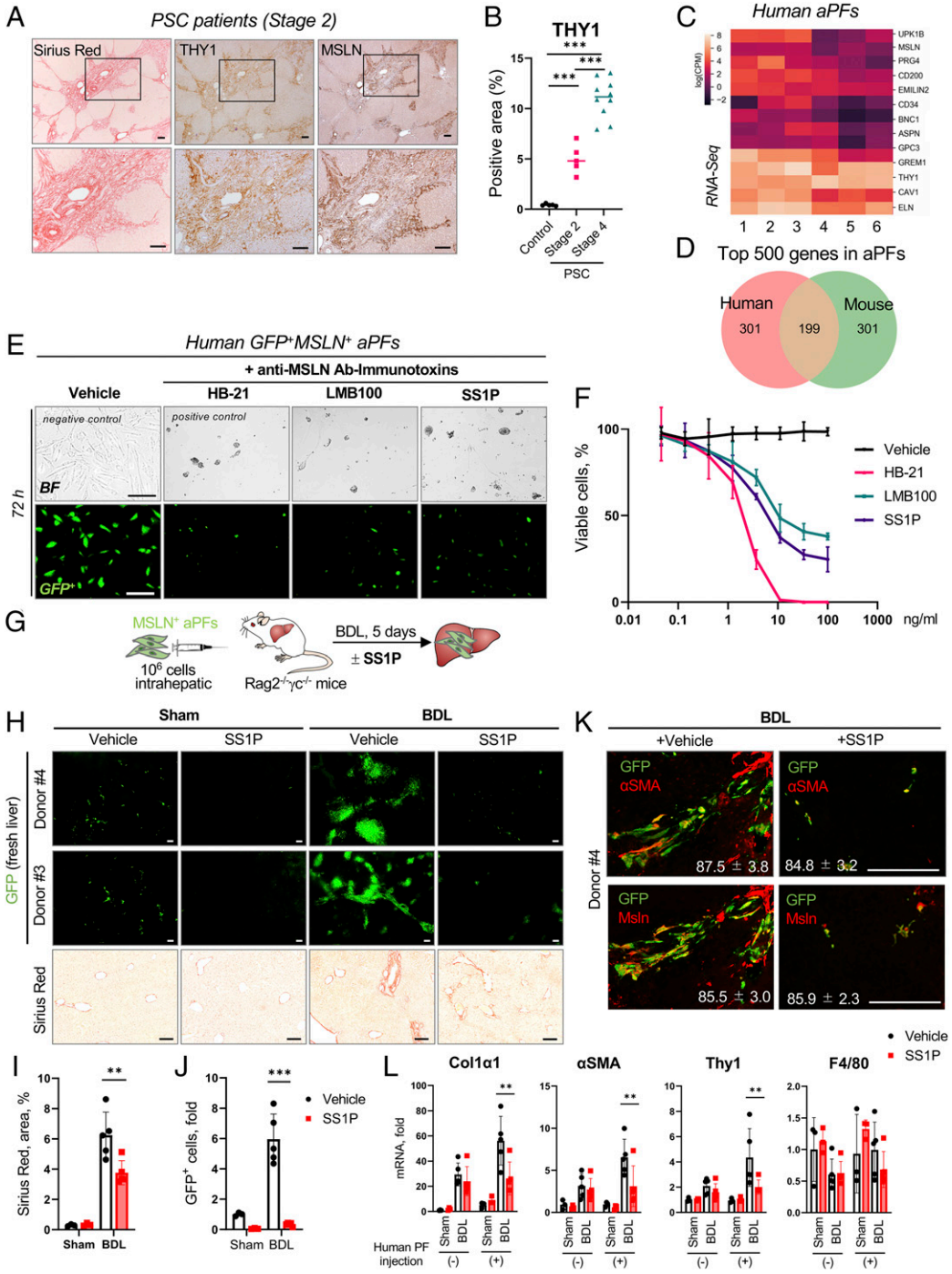


**Fig. 6.** Targeting human MSLN$^+$ aPFs using an anti-MSLN–based immunotoxin. (*A* and *B*) Resected livers from PSC patients (stage 2, $n = 5$; stage 4, $n = 10$) and healthy donors (control, $n = 5$) were stained with Sirius red, anti-human THY1, and MSLN Abs (*A*), and the correlation between the stage of PSC and Thy1-positive area was calculated as a percentage (*B*). (*C* and *D*) Primary human aPFs (from donors 1 to 6) were analyzed by RNA-seq. (*C*) Expression of selected markers in human aPFs is shown by heatmap [log(cpm)]. (*D*) Venn diagram depicting similarities between expression of the top 500 most highly expressed genes in human and mouse aPFs. (*E* and *F*) Human GFP-labeled aPFs were cultured ±anti-MSLN Ab immunotoxins SS1P (100 ng/mL) or LMB-100 (100 ng/mL), or anti-transferrin Ab immunotoxin HB-21 (positive control) vs. medium alone (negative control) for 72 h. (*E*) Bright-field (BF) and fluorescent micrographs. (*F*) The fit curve shows cell viability using a WST8 assay. (*G*–*K*) Humanized xenograft mice (generated by hepatic transplantation of human GFP$^+$MSLN$^+$ aPFs into livers of Rag2$^{-/-}$γc$^{-/-}$ mice) were sham- or BDL-injured, and treated with an anti-MSLN Ab immunotoxin (SS1P, 100 μg/kg, i.v., injected on days 1 and 3 post BDL; or vehicle, 0.2% human serum albumin) (*G*). (*H*) The whole-liver mount was analyzed using fluorescence microscopy (fluorescent micrographs); liver sections were stained with Sirius red (BF micrographs). (*I*) The positive area of Sirius red staining in the injected (left lateral lobe) was calculated as a percentage. (*J*) Liver sections were stained with DAPI, and the number of GFP$^+$DAPI$^+$ human aPFs was calculated in the injected lobe as a fold induction (vs. sham control mice). (*K*) Livers were stained for αSMA and MSLN, human aPFs were visualized by GFP expression, and the proportion of GFP$^+$αSMA$^+$/GFP$^+$ and GFP$^+$MSLN$^+$/GFP$^+$ cells was calculated as a percentage. (*L*) Expression of selected genes in the human aPF (–) liver lobes (median lobes) and human aPF (+) lobes (left lateral lobes) was analyzed by qRT-PCR. (Scale bars, 100 μm.) $^{**}P < 0.01$ and $^{***}P < 0.001$ by ANOVA.

tissue fibroblasts [via interaction with TGFβRI (4) or αv–β5 integrins (37)], while Msln facilitates TGFβ1–TGFβRI–pSmad2/3 signaling and FGF–FGFR/p-Akt–dependent proliferation of aPFs. In concordance, expression of Msln targets (TGFβRI, p-Smad2/3, and p-Akt) was reduced in $Msln^{-/-}$ tissue fibroblasts but up-regulated in $Thy1^{-/-}$ tissue fibroblasts. Moreover, expression of Msln was increased ∼8-fold in $Thy1^{-/-}$ tissue fibroblasts, suggesting that $Thy1^{-/-}$ mice should be highly susceptible to fibrosis. Paradoxically, liver/lung/kidney fibrosis was decreased by ∼50% in $Msln^{-/-}$ mice but only increased by ∼25% in $Thy1^{-/-}$ mice. We speculate that genetic deletion of the *thy1* gene results in blockade of Msln signaling, causing compensatory overexpression of Msln and its target genes. This effect could be associated with the loss of a Msln ligand (currently unknown), which is distinct from Muc16 (since Muc16 is dispensable for lung and kidney fibrosis).

Since its discovery in 1992 as a differentiation antigen that is also expressed in many cancers, the mechanism of MSLN signaling has remained unresolved. CA125 (mouse Muc16) is the only known ligand of MSLN and was reported to activate Src/Akt signaling in cancer cells (38, 39).

We have recently demonstrated that Msln can bind to Thy1 in aPFs. Both Msln and Thy1 are GPI-anchored proteins, which lack transmembrane domains, and can transmit their signals via the transmembrane receptors with or without intrinsic kinase activity (the latter requires recruitment of Src [focal adhesion kinase, FAK; Src-family kinase, SFK] or JAK protein kinases to their cytoplasmic domains) or via binding to the lipid raft proteins (such as caveolin-1 and MAL proteins) (40). Thus, Thy1 was shown to modulate lipid raft–associated signaling via the SFK and FAK pathways, promoting fibroblast adhesion and limiting migration (41). Other studies propose that Thy1 functions as a mechanosensor (42) that inhibits extracellular activation of tissue-associated latent TGFβ1 via interaction with αv–β5 integrins at the cell surface (37).

Targeting Msln may be beneficial for halting parenchymal organ fibrosis. Three classes of potential Msln inhibitors have been identified: anti-human MSLN immunotoxin (that causes the death of human $MSLN^{+}$ cancer cells) (23), anti–Msln-blocking Abs (43), or recombinant human soluble THY1 (that neutralizes Thy1 reactivity to αv–β5 integrins, TGFβRI, and possibly Msln) (20).

Although little is known about MSLN signaling, much progress has been made with immunotherapy-based therapeutics of human $MSLN^{+}$ malignancies. MSLN is differentially expressed between normal and cancer cells, thus making it a strong candidate for anticancer therapy (14). In this paper, we used the immunotoxins SS1P and LMB-100 to show depletion of mesothelin-expressing fibroblasts is beneficial. One drawback to SS1P and its successor LMB-100 is that immunotoxins contain a foreign protein and are immunogenic, limiting the number of treatment cycles that can be given (24, 26) (https://clinicaltrials.gov/ct2/show/NCT02810418). Fortunately, there are now several other anti-mesothelin agents including antibody–drug conjugates, bispecific antibodies, and CAR-T cells that can be used to kill mesothelin-expressing fibroblasts (14).

We hypothesized that anti-human MSLN Ab immunotoxins can target human aPFs (without disrupting liver architecture or liver function) (4). Expression of human MSLN and THY1 was up-regulated in livers of patients with PSC and correlated with the severity of cholestatic fibrosis. Similar to mouse aPFs, human aPFs expressed MSLN, THY1, and αSMA. Human aPFs actively contributed to fibrosis when adoptively transplanted into livers of adult immunodeficient $Rag2^{-/-}\gamma c^{-/-}$ mice, proliferated, and migrated to the portal areas in response to BDL injury. Here we demonstrate that targeting of human MSLN with SS1P resulted in ablation (>90%) of human aPFs (from two different patients) in livers of human xenograft mice. Despite the low ratio of engrafted human aPFs to endogenous mouse aPFs, our data suggest that immunotoxins can effectively cause apoptosis of human aPFs and attenuate development of cholestatic fibrosis. Generation of "human aPF xenograft" $Rag2^{-/-}\gamma c^{-/-}$ mice serves as a useful tool to study in vivo the variability of patient-specific responses of human aPFs (fibrogenic activation/proliferation) to specific MSLN inhibitors.

Overall, immunotherapy-based ablation of human aPFs/tissue fibroblasts might become a strategy for treatment of cholestatic fibrosis and fibrosis in other organs. It might not cure patients with cholestatic fibrosis but can decrease fibroproliferative responses to bridge PSC patients to liver transplantation or treatment of the etiological causes.

## Materials and Methods

**Mice.** Col-GFP (16), $Msln^{-/-}$ (11), $Muc16^{-/-}$ (44), $Thy1^{-/-}$ (8), and $Mdr2^{-/-}$ (6) mice, WT C57BL/6 male littermates, and $Rag2^{-/-}\gamma c^{-/-}$ mice (BalbC) were housed and maintained under specific pathogen-free conditions in a standard environment with a 12-h light–dark cycle and fed a diet of normal chow ad libitum at the animal facilities of the University of California San Diego under protocol S07088, approved by the Institutional Animal Care and Use Committee.

**Bleomycin-Induced Lung Fibrosis.** Anesthetized mice were orotracheally instilled with bleomycin (1 or 5 U/kg, or PBS, 100 μL; Fresenius Kabi). Lungs were collected 3 wk after bleomycin (1 U/kg) instillation (20).

**UUO-Induced Lung Fibrosis.** Mice were intraperitoneally anesthetized with ketamine (80 mg/kg) and xylazine (10 mg/kg), an abdominal midline incision was performed, and the right ureter was ligated (with 6-0 nylon) at two levels. Kidneys were collected after 2 wk of UUO; the nonobstructed contralateral (left) kidneys served as a control (45).

**Histological Analysis of Liver/Lung/Kidney Fibrosis in Mice.** Formalin-fixed paraffin-embedded mouse liver/lung/kidney sections were stained with hematoxylin and eosin (H&E), Sirius red, anti-Thy1.2 Ab (1:200; BioLegend; 105301), anti-αSMA Ab (1:200; Abcam; ab5694), anti–Pan-CK Ab (1:200; Dako; Z0622), anti-CD34 Ab (1:200; eBioscience, 14-0341-81; Abcam, ab81289), anti-Sox9 Ab (1:200; MilliporeSigma; AB5535), and anti-GFP Ab (1:300; Abcam; ab6673) followed by secondary Alexa Fluor 488– or 594–conjugated Abs (Invitrogen) or 3,3′-diaminobenzidine (DAB) staining (Vector Laboratories). Nuclei were visualized by DAPI. Images were taken using an Olympus microscope, the positive area was calculated as a percentage (using ImageJ), and representative images of >2 independent experiments are shown.

**Isolation of Primary Mouse aPFs and Lung and Kidney Fibroblasts.** Nonparenchymal cell fractions were isolated from livers of Col-$GFP^{+}Mdr2^{-/-}$, Col-$GFP^{+}Msln^{-/-}Mdr2^{-/-}$, Col-$GFP^{+}Muc16^{-/-}Mdr2^{-/-}$, and Col-$GFP^{+}Thy1^{-/-}Mdr2^{-/-}$ mice (12 wk old) using the pronase/collagenase method (4). Col-$GFP^{+}vitaminA^{-}$ aPFs were sort-purified from Col-$GFP^{+}vitaminA^{+}$ aHSCs using a FACSAria II (BD Biosciences). Lung fibroblasts were isolated from bleomycin-injured (1 U/kg, 3 wk) Col-$GFP^{+}$ (WT) and Col-$GFP^{+}Msln^{-/-}$ mice using 0.05% collagenase/0.05% trypsin/0.05% DNase digestion (37 °C, for 10 min) (46). Upon removal of the mesothelial capsule, kidney fibroblasts were isolated from UUO (2 wk)-injured Col-$GFP^{+}$ and Col-$GFP^{+}Msln^{-/-}$ mice using collagenase digestion of the renal cortex (47). Nonparenchymal single-cell suspensions were cultured (in Dulbecco's modified Eagle's medium [DMEM] + 10% fetal bovine serum [FBS]) for 6 h (to allow surface antigens to reexpress) and then stained with anti-Thy1.2-PE-Cy7 Ab (1:100; eBioscience; 250902-81); Col-$GFP^{+}Thy1^{+}$ and Col-$GFP^{+}Thy1^{-}$ lung and kidney tubular fibroblasts were sort-purified using a FACSAria II (BD Biosciences) and analyzed by RNA-seq and Western blotting.

**Western Blotting and Immunoprecipitations.** Mouse Col-$GFP^{+}Mdr2^{-/-}$ and Col-$GFP^{+}Mdr2^{-/-}Msln^{-/-}$ aPFs (4) and primary Col-$GFP^{+}$ and Col-$GFP^{+}Msln^{-/-}$ lung fibroblasts (46) were cultured ±TGFβ1 (5 ng/mL, 24 h; R&D Systems). Cell lysates or whole-tissue lysates (in lysis buffer: 50 mM Tris·HCl, pH 7.4, 250 mM NaCl, 10 mM Hepes, 0.5% Nonidet P-40, 2.5 mM 3-cholamidopropyl dimethylammonio-1-propanesulfonate, 10 mM NaF, 1 mM $Na_3VO_4$, 5% glycerol, 25 mM ethylenediaminetetraacetate, 2 mM ethylene glycol tetraacetic acid, 1 mM sodium deoxylate, plus protease inhibitor mixture) were analyzed by Western blotting using anti-αSMA (1:1,000; Abcam; ab5694), anti-Thy1 Ab (1:1,000; R&D Systems; AF7335), anti-Msln Ab (1:200; IBL; 28127), anti-TGFβRI Ab (1:1,000; Abcam; ab31013), and anti–p-Smad2/Smad2 Abs and anti–p-Akt/Akt Abs (1:1,000; Cell Signaling Technology; 3101/5339, 4060S/4691S), and normalized using anti–β-actin Ab (1:5,000; Sigma-Aldrich;

A5441). IPs: cell lysates were precleared at 4 °C/1 h with protein G Sepharose (MilliporeSigma) and incubated overnight with anti-Msln Ab (2 μg; IBL; 28127), anti-TGFβRI Ab (2 μg; Abcam; ab31013), or anti-Muc16 Ab (Abicode; R2334-3), and the collected immune complexes were analyzed by Western blotting using anti-Thy1 Ab, anti-Msln Ab, and anti-Muc16 Ab (1:500; Abicode; R2334-3).

**Livers from PSC Patients.** Deidentified archived formalin-fixed serial liver sections were obtained from liver transplant patients with PSC stage 2 ($n$ = 5) and 4 ($n$ = 10) liver fibrosis (Mayo Clinic, Institutional Review Board [IRB] 18-000798) or deidentified nonfibrotic livers declined for transplantation ($n$ = 5; approved project 171883XX; https://www.lifesharing.org) and immunostained with anti-αSMA Ab (1:100; Abcam; ab5694), anti-MSLN Ab (1:100; Abbiotec; 250519), and anti-THY1 Ab (1:100; Abcam; ab92574). Seven or more nonoverlapping images per field per patient were analyzed using ImageJ, and the positive area was calculated as a percentage.

**Isolation of Human aPFs.** Human aPFs were isolated from cholestatic livers declined for transplantation ($n$ = 6; IRB 171883XX; https://www.lifesharing.org). Upon removal of the common hepatic bile duct and dissection of the hepatic hilus, the intrahepatic biliary tracts (upright to the junction of the right and left hepatic ducts) were exposed, the segmental branches of intrahepatic ducts were dissected, and the nonparenchymal tissues surrounding the bile ducts were collected, minced (to 0.5 $mm^3$), digested using the collagenase/pronase method (48), filtered, and cultured (DMEM + 10% FBS) for 7 d, followed by cell sorting using anti–MSLN-PE Ab (49). Human $MSLN^+$ aPFs were phenotyped with anti-MSLN, anti-THY1, and anti-αSMA Abs, stimulated ±TGFβ1 (5 ng/mL, 24 h; Proteintech) ±Alk5 inhibitor (SB431542; 10 μM, 24 h; Selleckchem), and analyzed by RNA-seq and qRT-PCR. Selected human aPFs were labeled with GFP-lentivirus (LVP016-GP; GenTarget) (4).

**qRT-PCR.** qRT-PCR was performed using QuantStudio 3 (Applied Biosystems). Total RNA was isolated from livers, mouse aPFs and aHSCs, or human aPFs using TRIzol and the Pure Link RNA Mini Kit (Invitrogen). Expression levels of selected genes were calculated vs. the housekeeping gene HPRT using the ΔΔCt method (for primers, see *SI Appendix*, Tables S1 and S2). The data are relative mRNA levels compared with control.

**RNA-Seq.** RNA from mouse or human aPFs ($1 \times 10^6$ cells per donor, $n$ = 6) and mouse lung and kidney fibroblasts was subjected to RNA-seq according to standard protocols (Illumina). RNA-seq reads were aligned to the human (hg38) or mouse (mm10) genomes using STAR (50). Read quantification was performed using RSEM3 v1.3.0 and Ensembl annotation (Gencode version 19). Lowly expressed genes were filtered out (cpm >1 in at least one sample). Trimmed mean of M values (51) normalization was applied. The R BioConductor packages edgeR and limma (52) were used for the limma-voom (53) method for differential expression analysis. Relative expression heatmaps were constructed using the clustermap function from Python's statistical data visualization tool Seaborn (https://seaborn.pydata.org/). The log fold change was used to assess similarity between conditions with only one sample, by comparing the observed commonly up-regulated/down-regulated genes with what would be expected by chance given the observed fraction of up-regulated/down-regulated genes per condition (binomial test) at varying fold-change thresholds. Network analysis was conducted using the STRING web tool (54). Pathway analysis was conducted using the ToppGene Suite (55) and the g:Profiler Python tool (56).

**Anti-Human MSLN Ab Immunotoxins.** SS1P and LMB-100 were generated by conjugation of anti-human MSLN SS1P mAb (23, 24, 57, 58) to truncated *Pseudomonas* (PE38) exotoxin (25, 59). Cultured human aPFs were treated with SS1P or LMB-100 (0.05 to 100 ng/mL) for 72 h. Anti-transferrin Ab immunotoxin HB-21 was used as a positive control. Cell viability was measured using the WST-8 cytotoxicity assay (Dojindo).

**Humanized Xenograft Mice.** These mice were generated by intrahepatic transplantation of primary human $MSLN^+GFP^+$ aPFs into livers (left lateral lobes) of $Rag2^{-/-}gc^{-/-}$ mice. Mice were sham- or BDL-injured, and treated with anti-MSLN Ab immunotoxin (SS1P, 100 μg/kg, i.v., injected on days 1 and 3 post BDL; or vehicle, 0.2% human serum albumin). Livers were collected after 5 d of BDL, and liver fibrosis was analyzed in aPF-injected left lateral lobes (vs. noninjected median lobes).

**Statistics.** All data represent the mean ± SD. Comparisons of two groups were analyzed using an unpaired, two-tailed Student's $t$ test. Comparisons of three or more groups were analyzed using ANOVA. ANOVA with a Tukey–Kramer test was used for comparing multiple groups. Survival curves were determined using the Kaplan–Meier method, and groups were compared using the log-rank test. $P < 0.05$ was considered statistically significant. Analyses were performed using Prism (version 8.3.0; GraphPad Software).

**Data Availability.** All study data are included in the article and/or *SI Appendix*.

**ACKNOWLEDGMENTS.** We thank Ms. Karin Diggle for excellent technical assistance and Drs. Simon S. Wong, Thomas Whisenant, Katrin Hochrath, and Mojgan Hosseini (University of California San Diego) for help with experiments. This work was supported by NIH R01DK101737, U01AA022614, and R01DK099205, R01DK111866 (to T.K.), R01DK101737 (to D.A.B.), R01DK09920 (to D.A.B.), P50AA011999 (to T.K. and D.A.B.), and AI043477 (to D.A.B.). This research was supported in part by the Intramural Research Program of the NIH, National Cancer Institute, Center for Cancer Research.

1. K. N. Lazaridis, N. F. LaRusso, Primary sclerosing cholangitis. *N. Engl. J. Med.* **375**, 2501–2502 (2016).
2. J. A. Dranoff, R. G. Wells, Portal fibroblasts: Underappreciated mediators of biliary fibrosis. *Hepatology* **51**, 1438–1444 (2010).
3. K. Iwaisako *et al.*, Origin of myofibroblasts in the fibrotic liver in mice. *Proc. Natl. Acad. Sci. U.S.A.* **111**, E3297–E3305 (2014).
4. Y. Koyama *et al.*, Mesothelin/mucin 16 signaling in activated portal fibroblasts regulates cholestatic liver fibrosis. *J. Clin. Invest.* **127**, 1254–1270 (2017).
5. Y. Li, J. Wang, K. Asahina, Mesothelial cells give rise to hepatic stellate cells and myofibroblasts via mesothelial-mesenchymal transition in liver injury. *Proc. Natl. Acad. Sci. U.S.A.* **110**, 2324–2329 (2013).
6. J. J. Smit *et al.*, Homozygous disruption of the murine MDR2 P-glycoprotein gene leads to a complete absence of phospholipid from bile and to liver disease. *Cell* **75**, 451–462 (1993).
7. J. A. Gubbels *et al.*, Mesothelin-MUC16 binding is a high affinity, N-glycan dependent interaction that facilitates peritoneal metastasis of ovarian tumors. *Mol. Cancer* **5**, 50 (2006).
8. M. Nosten-Bertrand *et al.*, Normal spatial learning despite regional inhibition of LTP in mice lacking Thy-1. *Nature* **379**, 826–829 (1996).
9. J. Dudas, T. Mansuroglu, D. Batusic, B. Saile, G. Ramadori, Thy-1 is an in vivo and in vitro marker of liver myofibroblasts. *Cell Tissue Res.* **329**, 503–514 (2007).
10. M. I. Yovchev, J. Zhang, D. S. Neufeld, P. N. Grozdanov, M. D. Dabeva, Thymus cell antigen-1-expressing cells in the oval cell compartment. *Hepatology* **50**, 601–611 (2009).
11. T. K. Bera, I. Pastan, Mesothelin is not required for normal mouse development or reproduction. *Mol. Cell. Biol.* **20**, 2902–2906 (2000).
12. Y. Rinkevich *et al.*, Identification and prospective isolation of a mesothelial precursor lineage giving rise to smooth muscle cells and fibroblasts for mammalian internal organs, and their vasculature. *Nat. Cell Biol.* **14**, 1251–1260 (2012).
13. K. Chang, I. Pastan, Molecular cloning of mesothelin, a differentiation antigen present on mesothelium, mesotheliomas, and ovarian cancers. *Proc. Natl. Acad. Sci. U.S.A.* **93**, 136–140 (1996).
14. A. Rump *et al.*, Binding of ovarian cancer antigen CA125/MUC16 to mesothelin mediates cell adhesion. *J. Biol. Chem.* **279**, 9190–9198 (2004).
15. R. Hassan *et al.*, Mesothelin immunotherapy for cancer: Ready for prime time? *J. Clin. Oncol.* **34**, 4171–4179 (2016).
16. Y. Yata *et al.*, DNase I-hypersensitive sites enhance alpha1(I) collagen gene expression in hepatic stellate cells. *Hepatology* **37**, 267–276 (2003).
17. A. C. Cheung, M. J. Lorenzo Pisarello, N. F. LaRusso, Pathobiology of biliary epithelia. *Biochim. Biophys. Acta Mol. Basis Dis.* **1864** (4 Pt B), 1220–1231 (2018).
18. J. S. Hagood *et al.*, Loss of fibroblast Thy-1 expression correlates with lung fibrogenesis. *Am. J. Pathol.* **167**, 365–379 (2005).
19. G. Ramírez *et al.*, Absence of Thy-1 results in TGF-β induced MMP-9 expression and confers a profibrotic phenotype to human lung fibroblasts. *Lab. Invest.* **91**, 1206–1218 (2011).
20. C. Tan *et al.*, Soluble Thy-1 reverses lung fibrosis via its integrin-binding motif. *JCI Insight* **4**, 131152 (2019).
21. O. Kaneko *et al.*, A binding domain on mesothelin for CA125/MUC16. *J. Biol. Chem.* **284**, 3739–3749 (2009).
22. J. N. Schofield, T. W. Rademacher, Structure and expression of the human glycosylphosphatidylinositol phospholipase D1 (GPLD1) gene. *Biochim. Biophys. Acta* **1494**, 189–194 (2000).
23. R. Hassan *et al.*, Phase I study of SS1P, a recombinant anti-mesothelin immunotoxin given as a bolus I.V. infusion to patients with mesothelin-expressing mesothelioma, ovarian, and pancreatic cancers. *Clin. Cancer Res.* **13**, 5144–5149 (2007).
24. R. Hassan *et al.*, Phase 1 study of the antimesothelin immunotoxin SS1P in combination with pemetrexed and cisplatin for front-line therapy of pleural mesothelioma and correlation of tumor response with serum mesothelin, megakaryocyte potentiating factor, and cancer antigen 125. *Cancer* **120**, 3311–3319 (2014).

25. R. Hassan *et al*., Anti-tumor activity of K1-LysPE38QQR, an immunotoxin targeting mesothelin, a cell-surface antigen overexpressed in ovarian cancer and malignant mesothelioma. *J. Immunother.* **23**, 473–479 (2000).
26. R. J. Kreitman, R. Hassan, D. J. Fitzgerald, I. Pastan, Phase I trial of continuous infusion anti-mesothelin recombinant immunotoxin SS1P. *Clin. Cancer Res.* **15**, 5274–5279 (2009).
27. P. S. Chowdhury, I. Pastan, Improving antibody affinity by mimicking somatic hypermutation in vitro. *Nat. Biotechnol.* **17**, 568–572 (1999).
28. W. Liu *et al*., Recombinant immunotoxin engineered for low immunogenicity and antigenicity by identifying and silencing human B-cell epitopes. *Proc. Natl. Acad. Sci. U.S.A.* **109**, 11782–11787 (2012).
29. C. Alewine *et al*., Efficacy of RG7787, a next-generation mesothelin-targeted immunotoxin, against triple-negative breast and gastric cancers. *Mol. Cancer Ther.* **13**, 2653–2661 (2014).
30. I. Mederacke *et al*., Fate tracing reveals hepatic stellate cells as dominant contributors to liver fibrosis independent of its aetiology. *Nat. Commun.* **4**, 2823 (2013).
31. J. E. Eaton, J. A. Talwalkar, K. N. Lazaridis, G. J. Gores, K. D. Lindor, Pathogenesis of primary sclerosing cholangitis and advances in diagnosis and management. *Gastroenterology* **145**, 521–536 (2013).
32. P. Fickert *et al*., Regurgitation of bile acids from leaky bile ducts causes sclerosing cholangitis in Mdr2 (Abcb4) knockout mice. *Gastroenterology* **127**, 261–274 (2004).
33. S. L. Lin, T. Kisseleva, D. A. Brenner, J. S. Duffield, Pericytes and perivascular fibroblasts are the primary source of collagen-producing cells in obstructive fibrosis of the kidney. *Am. J. Pathol.* **173**, 1617–1627 (2008).
34. L. Barron, S. A. Gharib, J. S. Duffield, Lung pericytes and resident fibroblasts: Busy multitaskers. *Am. J. Pathol.* **186**, 2519–2531 (2016).
35. V. Gupta, I. Gupta, J. Park, Y. Bram, R. E. Schwartz, Hedgehog signaling demarcates a niche of fibrogenic peribiliary mesenchymal cells. *Gastroenterology* **159**, 624–638.e9 (2020).
36. R. Kramann *et al*., Perivascular Gli1$^+$ progenitors are key contributors to injury-induced organ fibrosis. *Cell Stem Cell* **16**, 51–66 (2015).
37. Y. Zhou, J. S. Hagood, B. Lu, W. D. Merryman, J. E. Murphy-Ullrich, Thy-1-integrin alphav beta5 interactions inhibit lung fibroblast contraction-induced latent transforming growth factor-beta1 activation and myofibroblast differentiation. *J. Biol. Chem.* **285**, 22382–22393 (2010).
38. U. Bharadwaj, C. Marin-Muller, M. Li, C. Chen, Q. Yao, Mesothelin confers pancreatic cancer cell resistance to TNF-α-induced apoptosis through Akt/PI3K/NF-κB activation and IL-6/Mcl-1 overexpression. *Mol. Cancer* **10**, 106 (2011).
39. M. C. Chang *et al*., Mesothelin enhances invasion of ovarian cancer by inducing MMP-7 through MAPK/ERK and JNK pathways. *Biochem. J.* **442**, 293–302 (2012).
40. K. Simons, J. L. Sampaio, Membrane organization and lipid rafts. *Cold Spring Harb. Perspect. Biol.* **3**, a004697 (2011).
41. J. E. Bradley, G. Ramirez, J. S. Hagood, Roles and regulation of Thy-1, a context-dependent modulator of cell phenotype. *Biofactors* **35**, 258–265 (2009).
42. V. F. Fiore *et al*., Conformational coupling of integrin and Thy-1 regulates Fyn priming and fibroblast mechanotransduction. *J. Cell Biol.* **211**, 173–190 (2015).
43. M. Onda *et al*., New monoclonal antibodies to mesothelin useful for immunohistochemistry, fluorescence-activated cell sorting, Western blotting, and ELISA. *Clin. Cancer Res.* **11**, 5840–5846 (2005).
44. D. J. Cheon *et al*., CA125/MUC16 is dispensable for mouse development and reproduction. *PLoS One* **4**, e4675 (2009).
45. R. L. Chevalier, M. S. Forbes, B. A. Thornhill, Ureteral obstruction as a model of renal interstitial fibrosis and obstructive nephropathy. *Kidney Int.* **75**, 1145–1152 (2009).
46. J. C. McIntosh, J. S. Hagood, T. L. Richardson, J. W. Simecka, Thy1 (+) and (–) lung fibrosis subpopulations in LEW and F344 rats. *Eur. Respir. J.* **7**, 2131–2138 (1994).
47. C. C. Sharpe, M. E. C. Dockrell, M. I. Noor, B. P. Monia, B. M. Hendry, Role of Ras isoforms in the stimulated proliferation of human renal fibroblasts in primary culture. *J. Am. Soc. Nephrol.* **11**, 1600–1606 (2000).
48. X. Liu *et al*., Identification of lineage-specific transcription factors that prevent activation of hepatic stellate cells and promote fibrosis resolution. *Gastroenterology* **158**, 1728–1744.e14 (2020).
49. A. Psyrri *et al*., Quantitative determination of nuclear and cytoplasmic epidermal growth factor receptor expression in oropharyngeal squamous cell cancer by using automated quantitative analysis. *Clin. Cancer Res.* **11**, 5856–5862 (2005).
50. A. Dobin *et al*., STAR: Ultrafast universal RNA-seq aligner. *Bioinformatics* **29**, 15–21 (2013).
51. M. D. Robinson, A. Oshlack, A scaling normalization method for differential expression analysis of RNA-seq data. *Genome Biol.* **11**, R25 (2010).
52. M. E. Ritchie *et al*., limma powers differential expression analyses for RNA-sequencing and microarray studies. *Nucleic Acids Res.* **43**, e47 (2015).
53. C. W. Law, Y. Chen, W. Shi, G. K. Smyth, voom: Precision weights unlock linear model analysis tools for RNA-seq read counts. *Genome Biol.* **15**, R29 (2014).
54. D. Szklarczyk *et al*., The STRING database in 2017: Quality-controlled protein-protein association networks, made broadly accessible. *Nucleic Acids Res.* **45**, D362–D368 (2017).
55. J. Chen, E. E. Bardes, B.J. Aronow, A.G. Jegga, ToppGene Suite for gene list enrichment analysis and candidate gene prioritization. *Nucleic Acids Res.* **37**, W305–W311 (2009).
56. J. Reimand *et al*., g:Profiler—A web server for functional interpretation of gene lists (2016 update). *Nucleic Acids Res.* **44**, W83–W89 (2016).
57. R. Hassan *et al*., $^{111}$Indium-labeled monoclonal antibody K1: Biodistribution study in nude mice bearing a human carcinoma xenograft expressing mesothelin. *Int. J. Cancer* **80**, 559–563 (1999).
58. R. Hassan, T. Bera, I. Pastan, Mesothelin: A new target for immunotherapy. *Clin. Cancer Res.* **10**, 3937–3942 (2004).
59. I. Pastan, R. Hassan, D. J. FitzGerald, R. J. Kreitman, Immunotoxin treatment of cancer. *Annu. Rev. Med.* **58**, 221–237 (2007).